SIAM J. APPL. MATH.
Vol. 48, No. 2, April 1988

POLYMER FLOODS: A CASE STUDY OF NONLINEAR WAVE ANALYSIS AND OF INSTABILITY CONTROL IN TERTIARY OIL RECOVERY*

PRABIR DARIPA†, JAMES GLIMM†‡, BRENT LINDQUIST†, AND OLIVER MCBRYAN†§

Abstract. Polymer flooding in oil reservoir simulation is considered in two space dimensions. The wave structures associated with such a process give rise to interesting phenomena in the nonlinear regime which have direct bearing on the efficiency of oil recovery. These waves influence and can prevent surface instabilities of the fingering mode. In this paper we resolve these waves by a front tracking method. We consider the fingering problem and the issue of oil recovery for the polymer flood. The details of these two phenomena depend on the separation between the waves and upon the viscosity contrast between the oil, water and polymer. We identify a nonlinear transfer of instability between adjacent waves and a nonlinear enhancement of recovery due to successive waves. The conclusions produced by this work are also pertinent to tracer flooding.

One interesting conclusion applies to polymer injection followed by pure water injection. In this case the instability is transferred to the polymer-water interface, and the pure water region can break through the polymer to achieve direct contact with the oil. The polymer is left in narrow ribbons parallel to the main flow field and is by-passed by pure water. The effect of narrow regions of by-passed polymer can be simulated by the front tracking method and is not equivalent to numerical or physical diffusion, which would distribute the polymer more uniformly and retard the breakthrough of water through the polymer layer.

Key words. hyperbolic equations, front tracking, Riemann problem, flow in porous media, polymer displacement, nonlinear waves, tertiary oil recovery

AMS(MOS) subject classifications. 76S05, 65M99, 35L65, 35L67, 35B35

1. Introduction.

Polymer flooding of oil reservoirs is known to be an effective method of tertiary oil recovery [38], [41]. Such a process involves injection of water thickened with polymer (possibly after the reservoir has been flooded with pure water during a secondary recovery phase). Since a polymer-thickened aqueous phase is more viscous than pure water, an increase in the net oil recovery is achieved through (1) inhibition of the growth rate of the fingering instability and (2) an increase of the saturation level behind the polymer-treated aqueous bank. The study of these two effects is the subject of this paper, namely instability control and nonlinear wave analysis. We consider banks formed in the displacement process to be interfaces across which the aqueous saturation and/or the polymer concentration effectively change discontinuously. The polymer model studied here gives rise to a rich wave structure in the flow field including several such discontinuity interfaces as well as smoothly varying rarefaction waves. The recovery properties of the polymer flood can be understood in terms of this wave structure and its relation to the parameter space of the problem. We perform a study of the fingering instability for the interfaces present in the polymer flood. See [5] for a treatment of a related problem in stratified Hele-Shaw flow.

* Received by the editors December 1, 1986; accepted for publication (in revised form) March 27, 1987.

† Department of Mathematics, Courant Institute of Mathematical Sciences, New York University, New York, New York 10012. The work of this author was supported in part by the Applied Mathematical Sciences subprogram of the Office of Energy Research, U.S. Department of Energy, under contract DE-AC02-76ER03077.

‡ The work of this author was supported in part by the Army Research Office grant DAAG29-85-0188 and the National Science Foundation grant DMS-83-12229.

§ Center for Theory and Simulation, Cornell University, Ithaca, New York 14853. Permanent address, Courant Institute of Mathematical Sciences, New York University, New York, New York 10012. The work of this author was supported in part by National Science Foundation grant DMS-83-12229.

Front tracking, as developed by the authors and co-workers [9], [14]-[22] is the numerical method used in this study. The idea of this method is to use a moving lower dimensional grid (a system of curves in two dimensions) to represent solution discontinuities. The method uses analytic or asymptotic solutions directly within the computational process; these tools give extraordinarily sharp resolution to the dominant solution features. This is accomplished by the use of mathematical analysis and physical understanding directly within the computational algorithm.

This circle of ideas has been applied in other contexts, usually where solutions of high quality are of critical importance and where conventional difference methods, which excel for smooth solutions, perform poorly. For example, we note that the dominant engineering code for the study of deformations in metals at high strain rates uses master-slave interfaces to resolve shear bands [27], [44]. The only satisfactory numerical treatment of moving artificial heart valves [39] uses moving points to represent the valve position. A complicated flow pattern about a convex body was given in [49] using front tracking methods. Several interface methods have been developed for two fluid, incompressible Euler flow. Besides the more general front tracking approach [23], we mention various pure interface methods, such as boundary integral methods and vortex methods [6], [7], [29], [33], [47] and complex variable methods [34]. A simplified early version of front tracking was successfully combined with adaptive grid methods [12]. Hoegh-Krone and co-workers also report progress with front tracking in two dimensions [24]. The one-dimensional front tracking code of Swartz and Wendroff [45] has given the only satisfactory solution of the Noh problem [36]. Plohr's one-dimensional tracking [40] has given three orders of magnitude improvement in the accuracy of the solution of the McCall [32] problem. P. Charrier and B. Tessieras [8] write, with reference to their one-dimensional front tracking method, "The quality of the results obtained by front tracking schemes (high resolution in discontinuity, high precision in regular zones, no dissipation in the shock) justifies interest in the method." The contributions of Lazarus [31] should also be cited.

A list of what has been regarded as the essential scientific obstacles to front tracking was given in [9]. At the time of the writing of that paper and especially since then, many of these obstacles have been overcome. It seems correct to state that the scientific proof of principle for front tracking as a generic method for adaptive resolution of solution discontinuities has been achieved, in large part due to the work of the authors and co-workers, and that this proof of principle has been confirmed by subsequent investigations of a number of other workers on a wide range of problems. It was preceded by the adaptation of this method to specific computations by several workers, in particular Richtmyer and Morton [43] and Moretti [35].

The paper is organized as follows. In § 2 the governing equations of the polymer flooding process are presented. In § 3 the wave structure associated with the polymer flooding process is briefly described and some complications for front tracking algorithms implied by this wave structure are discussed. The results of our numerical experiments on core floods and quarter five-spot geometries appear in § 4.

2. The polymer model. A model of a polymer flood process in which the polymer acts solely as a device for controlling the viscosity of one of two incompressible, immiscible phases (which we refer to as the aqueous and oil phases) is described by the following system [25], [41]:

$$s_t + \nabla \cdot (\vec{v} f(s, c)) = \text{source terms}, \tag{1a}$$

$$(sc)_t + \nabla \cdot (\vec{v} c f(s, c)) = \text{source terms}, \tag{1b}$$

(1c) $$\nabla \cdot \vec{v} = \text{source terms},$$

(1d) $$\vec{v} = -\lambda(s, c)\nabla p.$$

Here s is the saturation (volume fraction) of the aqueous phase, c is the concentration of polymer added to the aqueous phase, $\vec{v}$ is the total seepage velocity, p is the pressure, $\lambda(s, c)$ is the total mobility, and $f(s, c)$ is the fractional flow function relating the aqueous seepage velocity to the total seepage velocity.

Equations (1a) and (1b) are, respectively, the mass conservation laws for the aqueous phase and the polymer, (1c) is the incompressibility condition, and (1d) is Darcy's law relating the total seepage velocity to the pressure gradient. In this model, the polymer has been assumed to be completely miscible in the aqueous phase and completely immiscible in the oil phase. Further, the following effects have been neglected: volumetric swelling of the aqueous phase with added polymer, diffusion of the polymer, adsorption of the polymer onto the reservoir rock, capillarity and gravity. For a model of polymer flooding with adsorption effects included see [26]. The reservoir is assumed to be homogeneous, although this restriction is relaxed in § 4.2.

The total mobility λ and the fractional flow function f are defined as

(2) $$\lambda(s, c) = \lambda_0(s) + \lambda_a(s, c), \qquad f(s, c) = \lambda_a(s, c)/\lambda(s, c),$$

where $\lambda_0(s)$ and $\lambda_a(s, c)$ are, respectively, the mobilities of the oil and aqueous phases. For our purposes the mobilities are taken as follows:

(3) $$\lambda_a(s, c) = \frac{s^2}{\nu_a(c)}, \qquad \lambda_0(s) = \frac{(1-s)^2}{\nu_0}.$$

The quantities $\nu_a(c)$ and ν_0 are, respectively, the viscosities of the aqueous and oil phases. We assume the viscosity of the aqueous phase depends linearly on the polymer concentration

(4) $$\nu_a(c) = \nu_w(1 + \mu c),$$

where ν_w is the pure water viscosity and the coefficient μ characterizes the particular polymer used as a thickening agent.

In many core flood studies the injection of tracer particles along with an aqueous phase is also of practical interest. Tracer particles do not change the phase viscosities, so the model (1)-(4) with $\mu = 0$ describes injection of tracer particles of concentration c. Equation (1b) becomes decoupled from system (1) and the tracer particles are advected passively with the background water flow. The waves which arise in tracer flow are the same as for the polymer problem. Front tracking therefore provides a method of following these tracer fronts without numerical diffusion.

3. The solution of the Riemann problem. The front tracking algorithm has been extensively described elsewhere [18], [20], [22]. It requires the solution of the Riemann problem (RP) for the hyperbolic system (1a), (1b) in order to advance the tracked discontinuities in the solution. In two space dimensions, as considered here, the propagation of a tracked discontinuity is achieved by local splitting of the hyperbolic operator in normal and tangential directions. As the solution is smooth in the tangential direction on each side of a discontinuity, it suffices to look at the RP solution in one space dimension, corresponding to an analysis of the propagation of the discontinuity in the normal direction. Equations (1a) and (1b) in one space dimension can be written as

(5) $$s_t + (sg(s, b))_x = 0, \qquad b_t + (bg(s, b))_x = 0,$$

where $b = sc$ is the polymer volume fraction, and $g(s, b) = f(s, b)/s$ is the water particle velocity. For the study of the RP solution, the seepage velocity $\vec{v}$ and the source terms in (5) have been respectively set to one and zero without any loss of generality. The global existence of a solution to the above system for arbitrary, but nearly constant, initial data has been proven in [46] and the RP solution can be found in [25], [28]. We briefly review the solution here.

The wave structure of the above system can be understood in terms of the waves associated with the flooding of a reservoir by pure water. For the case of one-dimensional flooding of a reservoir by pure water, the hyperbolic equation is a single scalar conservation law

$$s_t + (f(s))_x = 0, \tag{6}$$

the familiar Buckley–Leverett equation. For the case of a nonlinear fractional flow function $f(s) \in C^2$ having at most a finite number of inflection points (as in immiscible flow), the Riemann problem solution is described in terms of a single family of waves consisting of both rarefaction waves (across which s varies smoothly) and shock waves (across which s varies discontinuously). For the case of a fractional flow function linear in s (as in miscible flow), the RP solution consists only of contact discontinuities, across which s jumps discontinuously. No smoothly varying region can occur for the saturation field in miscible flow unless it is present in the initial data.

The Riemann problem solution to (5) is constructed by using the elementary waves associated with the system. There are two families of waves, referred to as the C and S families. The smoothly varying waves (rarefactions) are found by rewriting (5) as

$$U_t + A(U)U_x = 0, \tag{7}$$

where $U \equiv (s, b)$ and $A(U)$ is the Jacobian matrix:

$$A(U) \equiv \frac{\partial(sg(s, b), bg(s, b))}{\partial(s, b)}. \tag{8}$$

The eigenvector fields e^C and e^S, and corresponding eigenvalues λ^C and λ^S, of $A(U)$ then determine the rarefaction wave structure. The discontinuous waves (shocks) are obtained from the jump conditions which are a generalization of the Rankine–Hugoniot relation.

The S family of waves is identical to that obtained for the immiscible case described above. It consists of rarefaction waves and shocks across which s changes, continuously and discontinuously respectively, but across which $c = b/s$ remains constant.

The C family is a degenerate field, analogous to the case of miscible flow mentioned above, consisting solely of contact discontinuities. Across the contact discontinuity, both s and c change such that the function $g(s, b)$ remains constant. Since the polymer is completely miscible in water, there can be no smooth variation in polymer concentration unless such variation is present in the initial data. The functions $c(s, b)$ and $g(s, b)$ are, respectively, referred to as the Riemann invariants of the S and C fields.

For a system of equations that are strictly hyperbolic, the waves passing through any point in phase space can be strictly ordered according to their corresponding speeds. For the polymer flood (5), there is a line in phase space, the transition line τ, along which the speeds of the S and C families of waves are identical. Hence the system (5) fails to satisfy the condition of strict hyperbolicity and a generalized entropy condition due to Lax [30] is applied to obtain a unique solution. One consequence of this failure of strict hyperbolicity is that no two states that lie on opposite sides of the transition line in phase space can be connected solely by a contact discontinuity of the C family.

The solution to a Riemann problem in one space dimension can be described as the traversal of phase space $\{U \equiv (s, c)\}$ from a left state U_L to a right state U_R.[1] The path in phase space consists of a sequence of elements each of which has physical manifestation as an elementary wave in the t, x plane. The reader is referred to [25] for the exact construction of the phase space path from any left state (s_L, c_L) to any right state (s_R, c_R) for the RP solution to (5). We comment here on the two cases of interest for the numerical studies described in § 4. Consider the RP for which the right state U_O is pure oil ($s_O = 0$, $c_O = 0$) and the left state U_P is an aqueous state of nonzero polymer concentration. The solution path in phase space (Fig. 3.1) contains, in addition to other waves, a C-contact and an S-shock which travel at the same speed. If, however, the right state contains connate water ($s_O \neq 0$) the two discontinuities split with the S-shock travelling faster. Thus an intermediate layer of polymer free water tends to separate a right state U'_O with $s'_O \neq 0$, $c'_O = 0$ from a left state U_P with $s_P \neq 0$, $c_P \neq 0$. The second case consists of the RP describing the transition from a left state of pure water $U_W = (1, 0)$ to the polymer-thickened aqueous state U_P defined above. The solution path in phase space (also shown in Fig. 3.1) consists of an S-wave rarefaction fan from the state U_W to an intermediate state $U^{**} = (s^{**}, 0)$ and a C-contact discontinuity from U^{**} to U_P.

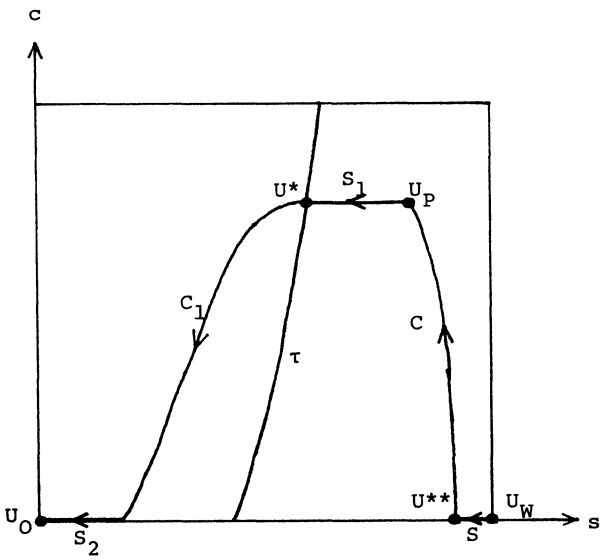

FIG. 3.1. *Two solution paths in phase space*: (a) *from a left state U_P describing a polymer thickened aqueous phase typical to reservoir tertiary-recovery practices, to a right state U_O describing a state of pure oil. The C- and S-shocks described respectively by the paths designated C_1 and S_2 travel at the same speed.* (b) *from a left state U_W describing pure water, to a right state U_P as in* (a). *The transition line is labelled τ.*

The greater complexity of the wave structure of the Riemann problem solution for the polymer flood complicates the problem of labelling and identifying the waves in a tracking algorithm. Since currently only the discontinuity waves are tracked, in the discussion that follows we shall refer only to shocks of the S and C families.

[1] Although the fundamental variables for the conservation form (5) are s and b, the solution is drawn easiest in (s, c) space.

The Riemann problem solution for (5) can contain at most one C-contact and two S-shocks (for the case of quadratic permeability functions used in (3)). While identification of the C-contact is unambiguous, each S-shock must be further labelled before it can be uniquely identified. There does not appear to be a logically consistent global label, holding for all time and all points on an S-shock once it has been created, to uniquely identify an S-shock. This is particularly true in flows where shocks begin to interact with each other or move under the influence of nonconstant reservoir conditions, i.e., flow hysteresis induced by varying directions of flooding. We propose that a local labelling system is required, one that can change spatially along any given wave front and in time.

We present an abstract formulation of this problem. Let $\mathcal{S}$ be the state space, or the space of dependent variables for the system (5). For an $n \times n$ system, $\mathcal{S} \subset \mathcal{R}^n$. Then a wave family can be regarded as an $n+1$ dimensional surface contained in $\mathcal{S} \times \mathcal{S}$, defined by the set of all pairs (U_L, U_R) connected by this family of waves. There are two connected surfaces, defining the S- and C-waves. However, no finer global distinction between S-waves can be imposed, as all S-waves can be continuously deformed into one another. Thus further labelling has the character of local coordinate systems on a manifold and must be done by overlapping charts. Similar problems arise in the scalar Buckley–Leverett flow with gravity, where two inflection points in the flux function allow a double shock to occur within the single mode of the problem [42]. Some nonconvex stress–strain relations in elasticity give rise to a similar shock splitting. Shock splitting within a single mode is observed also in the elastic–plastic regime of strong shock waves in metals.

One such proposal for the polymer flood would use the orientation of the total seepage velocity as a label, since the flow direction can be reversed along a given shock front, either at distinct times or at distinct points at the same time. Given the velocity orientation at a point on the shock front, each side of the shock at this point can be uniquely labelled as the *ahead* or *behind* side. A point on an S-shock would then be referred to as a point of direct (back) flow if the saturation decreases (increases) as the shock is crossed from the behind to the ahead side. Analysis of all possible Riemann problem solutions for the polymer flood show that at most one back flow S-shock will appear. However, two direct flow S-shocks can appear in the solution but are distinguished by their ahead and behind side states. The ahead and behind states for a direct flow S-shock will either lie solely to the left of, or solely to the right of, the transition line in phase space. In either case one state may lie on the transition line. Thus a complete labelling system for the discontinuity waves would involve a quadruple of labels for each point of a tracked shock: namely its family affiliation (S or C); its flow direction, which can be specified relative to the tangent vector $\vec{t}$ of the oriented discontinuity curve as sgn $(\vec{v} \times \vec{t} \cdot \hat{z})$, where $\hat{z}$ is the unit vector out of the computational plane; the orientation $\mathcal{O}$ of the solution gradient with respect to the total fluid velocity, namely $\mathcal{O} = \text{sgn}\,(-\nabla s \cdot \vec{v})$ usually referred to as direct flow for positive $\mathcal{O}$ and backwards flow for negative $\mathcal{O}$; and, for the case of direct flow S-shocks, a position designation in phase space (left or right of the transition line τ). Such issues are not important for the constant flow studies done here.

4. Results. Three sets of calculations were performed using the polymer model described above. The first series of calculations studied the development of single fingers in polymer floods of rectangular cores. The second series studied the growth of fingers and oil recovery efficiency in quarter five spot floods of homogeneous reservoirs. The final series compared the fingering and recovery behavior as a function

of increasing polymer concentration in quarter five spot floods of heterogeneous reservoirs.

4.1. Fingering in core floods. There is a transfer of instability between adjacent fronts in reservoir recovery processes. In addition, a succession of fronts produces recovery levels different from those anticipated by a study of single fronts alone. Both phenomena are aspects of nonlinear wave coupling and interactions which we explore in the present section.

It is useful for further analysis to understand the growth rates of S- and C-waves in isolation which arise in the polymer problem. A C-wave in isolation is identical to the Hele-Shaw interface which has been extensively studied [1]-[4], [13], [37], [48] and will not be discussed here. We first discuss the growth and recovery behavior of single fingers in isolation for the S-wave. We consider the displacement of pure oil by pure water—a process occurring via an S-wave shock followed by an S-wave rarefaction fan. The calculations are done in a slab core flood geometry, a rectangular domain $x \in [0, X]$, $y \in [0, Y]$, with no-flow boundaries on the sides $y = 0, Y$, inflow at the lower boundary $x = 0$ and outflow at $x = X$.

The stability of an S- or C-wave discontinuity is governed by the frontal mobility ratio, M_f,

$$M_f \equiv \frac{\lambda(s_B, c_B)}{\lambda(s_A, c_A)}, \tag{9}$$

where $\lambda(s, c)$ is defined in (2) and the states (s_B, c_B) and (s_A, c_A) are respectively defined immediately behind and ahead of the discontinuity. The dependence of M_f^C (for the C-wave discontinuity) and M_f^S (for the S-wave shock) on the viscosity ratio

$$r \equiv \frac{\nu_A}{\nu_B} \tag{10}$$

is shown in Fig. 4.1 for the system (1)-(4). M_f^S and M_f^C have the following properties:

$$M_f^S \leqq 2 \quad \text{for } 0 < r < \infty,$$

$$M_f^S = 1 \quad \text{for } r = 3 \quad (\text{assuming } S_A = 0, S_B = 1),$$

and

$$M_f^C = r,$$

$$M_f^C = 1 \quad \text{for } r = 1.$$

The critical mobility ratio $M_f = 1$ marks the limit of stability for planar S and C shocks to a small amplitude disturbance connecting two piecewise constant states. Since the linearized growth rate is proportional to $(M_f - 1)$ (see [11], [14], [19]) and M_f^C is unbounded, the C-wave can be more unstable than the S-wave. To understand the nonlinear wave coupling of S- and C-waves, we first consider the large amplitude instability of S-waves (also see [10], [14]) over a range of control parameters to which the linearized theory does not apply. (As mentioned earlier the C-wave is analogous to the Hele-Shaw interface for which the reader is referred to [1]-[4], [13], [37], [48].)

In Fig. 4.2, we show the development of a single S-wave finger over a sequence of times. It corresponds to the displacement of pure oil by pure water for the case $r = 10$ $(M_f^S = 1.4)$. The initial sine wave perturbation has its amplitude equal to its wavelength. In Fig. 4.2 and all subsequent relevant figures, the amplitude (height) of a perturbation finger shall be measured normalized with respect to its initial wavelength,

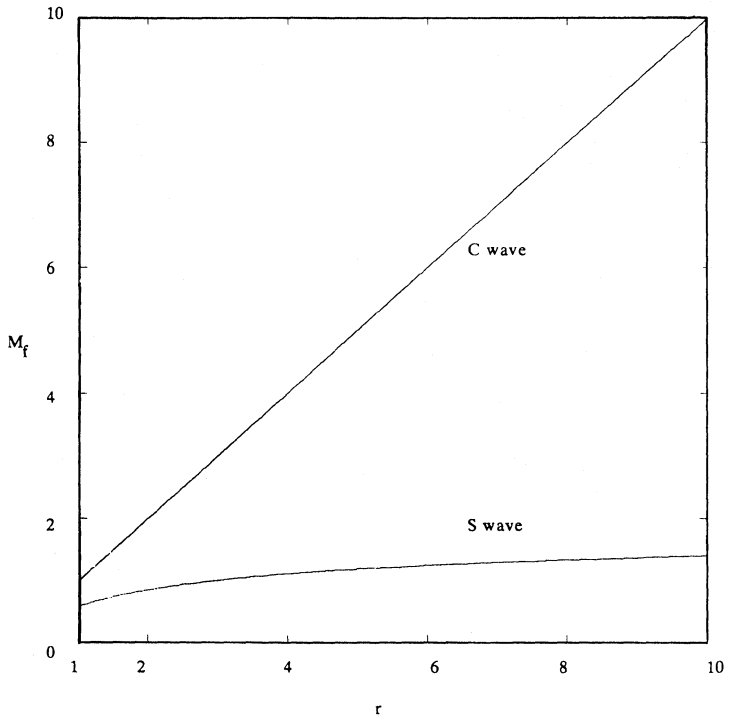

FIG. 4.1. *The frontal mobility ratio M_f for the S-wave and C-wave shocks of the polymer model as a function of viscosity ratio r of the fluid ahead of the front to that behind the front.*

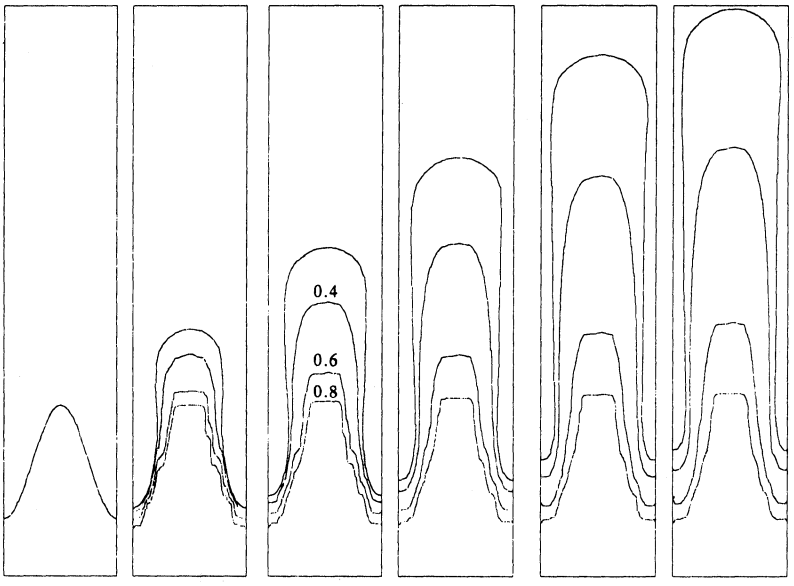

FIG. 4.2. *Growth of fingers in immiscible flow: The leftmost frame shows the initial interface separating two constant states of $S=1$ ahead and $S=0$ behind. Successive frames show the time development of this interface and the rarefaction waves behind this leading interface which is an S-shock. Level curves of saturation in the rarefaction zone are shown for three values of saturation. The initial viscosity ratio of the behind to ahead fluid is* 1:10.

which for all calculations shown here is the width of the calculational domain. The plots also show the S-wave family rarefaction fan which develops and trails behind the leading S-wave shock defining the finger. The contours for saturations equalling 0.8, 0.6 and 0.4 are given in each plot. In Fig. 4.3 we plot the finger growth versus fractional area behind the front for several values of r. The initial growth is seen to be linear in time in this large amplitude regime, rather than the exponential growth found in the linear (small perturbation) regime. The front is unstable even for $M_f < 1$ (see the curve for $r = 2$, $M_f = 0.845$), the finger achieving a finite growth in finite time.

We now consider displacement by a succession of two interfaces and contrast the growth and recovery behavior to that of single interfaces acting in isolation. For the calculations shown here (pure oil displaced by a layer of polymer-thickened water followed by the continued injection of pure water) the discontinuity separating the pure oil from the polymer-thickened water consists (as mentioned in § 3) of an S-wave shock and a C-wave contact discontinuity travelling at precisely the same speed. It is important to realize, however, that as long as the saturation ahead of this composite discontinuity remains zero, the composite wave acts *exactly as if it consisted of a single S-wave shock for a water–oil displacement flood of a viscosity ratio r closer to unity.* For this reason we shall refer to the leading discontinuity in the remainder of this discussion as an S-wave shock. The trailing discontinuity separating the polymer-thickened water layer from the pure water is a C-wave contact discontinuity.

Assume the properties of the fluids ahead of the S-wave and behind the C-wave remain fixed. There remain two essential parameters in this problem. The first is the dimensionless separation between the two discontinuities. The influence of one discontinuity on the other will be a decreasing function of separation between them. When

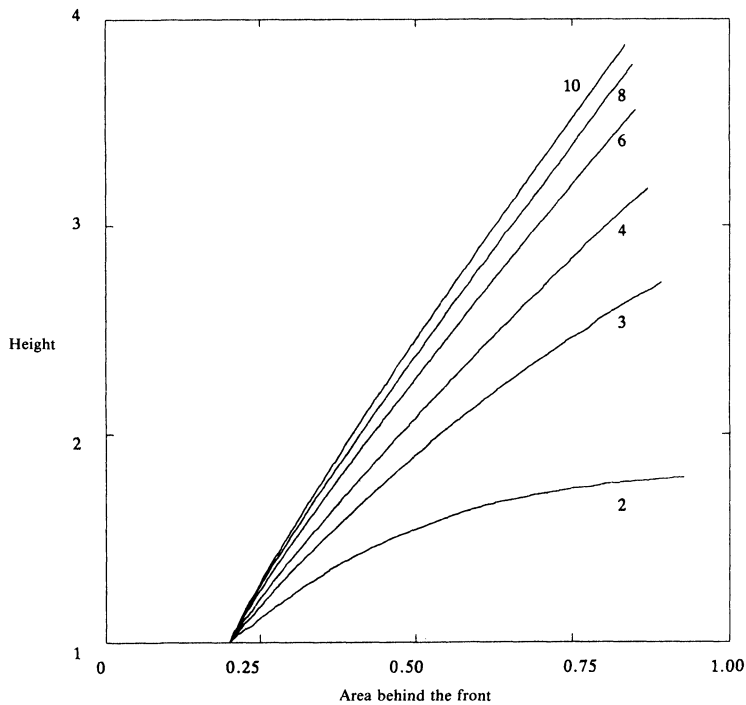

FIG. 4.3. *Finger height (normalized wrt wavelength) as a function of area behind the front for different values of viscosity ratio across an S-wave discontinuity.*

the separation is sufficiently large, the stability of each discontinuity is independent of the other and is governed by individual growth rates. When the separation becomes small enough, the stability of the combined interfaces is effectively governed by a single mobility ratio M_{eff} defined as the ratio of mobilities for the fluid immediately behind the C-wave to the fluid immediately ahead of the S-wave. The second essential parameter is the viscosity of the intermediate fluid between the discontinuities. An increase in the viscosity of the intermediate fluid, caused by an increase of the polymer concentration, makes the forward S-wave discontinuity more stable and makes the C-wave discontinuity less stable. Thus in the two interface problem, there is a level of instability, which can be transferred from one interface to another by a change in the properties of the intermediate fluid.

From these two observations, one predicts the following behavior for the unstable regime of the two interface problem under consideration. The more unstable C-wave will finger with a higher velocity than the S-wave ahead of it, overtake the leading discontinuity, after which the two waves interact and move as a composite, with a growth rate determined by the fluids in the extreme (ahead and behind) locations.

This overtake and breakthrough of the pure water region behind the C-wave occurs at the tip of the finger. Away from the tip, the polymer-thickened aqueous phase is left in narrow ribbons parallel to the flow field and thus becomes by-passed, making the polymer presence effectively useless. This effect is captured nicely by the front-tracking method. As the phenomenon is due to nondiffusive effects, finite difference methods introducing numerical diffusion would tend to distribute the polymer more uniformly and consequently predict a greater retardation in the time of breakthrough of the C-shock through the polymer layer.

We consider a two interface calculation in the same geometry as the single interface calculations above. The viscosity ratio of the top (oil), middle (polymer-water) and bottom layer (pure water) is 10:2:1. The initial dimensionless separation (normalized with respect to the wavelength of the initial perturbations) between the two interfaces is $\frac{1}{2}$. In Fig. 4.4 we show a sequence of the S- and C-wave discontinuity positions tracing a history of successive times in the calculation. For clarity, the rarefaction fans that develop between the two discontinuities and in the region of the finger behind the C-wave have been suppressed in this figure. In Fig. 4.5 we plot the saturation contour levels 0.8 and 0.6 as well as the interface positions for the solution at a single time. From the linear stability analysis and the calculations on single interfaces, the C-wave ($M_f = 2$) is expected to be more unstable than the S-wave ($M_f = 1.18$) and the predicted behavior of overtake, interaction and subsequent movement as a single unit at the tip is seen to occur (Fig. 4.4).

In Fig. 4.6 we summarize the growth rates expected for the one extreme of widely separated S- and C-wave interfaces and for the other extreme of a single, interacting, composite formed after overtake. The figure plots the mobility ratio for these three interfaces as a function of the viscosity of the intermediate layer (the frontal mobility ratio of the composite wave is the effective mobility ratio when the interfaces have zero separation). Figure 4.6 suggests that an increase in the separation between the two waves for fixed values of the viscosities should have considerable stabilizing effect on the S-wave and a milder destabilizing effect on the C-wave. This is indeed observed for the large amplitude case as shown in Fig. 4.7 where the growth rates of the S- and C-waves are plotted for various values of initial separation between the interfaces at a fixed value of viscosity ($\nu_{wp} = 6$) for the intermediate polymer zone. Over the range of separations studied here, the effect on the growth rate of the C-wave is unnoticeable, but a large stabilizing effect on the S-wave is seen.

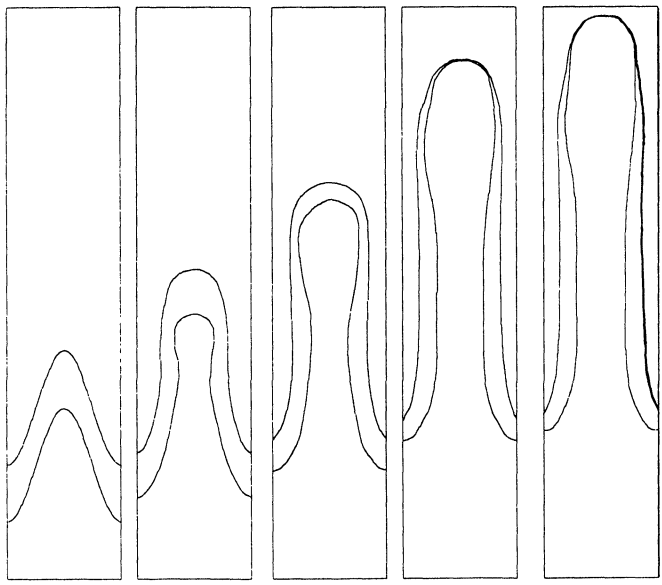

FIG. 4.4. *Large amplitude simulation for S- and C-shocks: stages in the temporal evolution of the S- (leading interface) and C-waves. The leftmost frame shows the initial position of two interfaces separating three layers of constant states. Only the middle layer contains polymer. The viscosity ratio for the three layers from bottom to top is* 1:2:10 *and the initial separation between the waves is half the wavelength of the initial perturbation.*

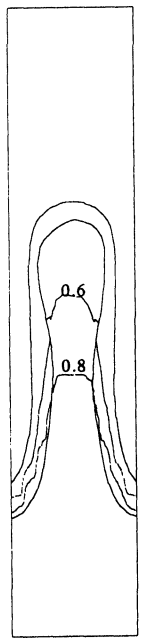

FIG. 4.5. *Contour plots of saturation for the third frame of Fig.* 4.4. *For clarity, only two saturation contours are shown in addition to the leading and trailing shocks.*

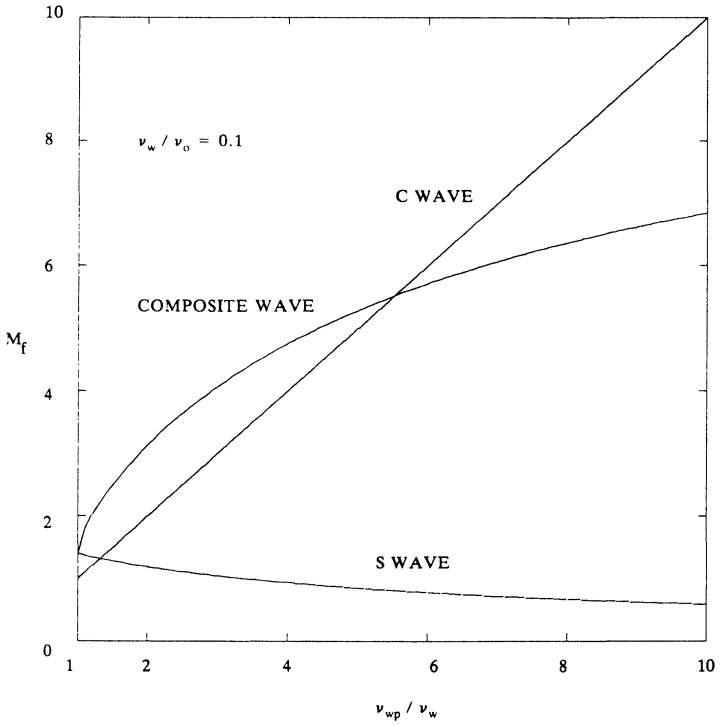

FIG. 4.6. *The frontal mobility ratio of the S-wave, C-wave and composite wave (see text) as a function of the viscosity of the intermediate polymer zone.*

We now consider the effect of the second parameter, the viscosity of the intermediate polymer zone. In Fig. 4.8 we plot the growth of the S (leading interface) and the C (trailing interface) waves for different values of the viscosity of the intermediate polymer zone. The left and right branch in each of these figures correspond to initial dimensionless separation between the waves, i.e., initial thickness of the polymer zone of 1 and 2, respectively. An increase in the viscosity of the intermediate layer has a stabilizing effect on the S-wave and a destabilizing effect on the C-wave, consistent with expectations.

The growth rates of the S- and C-waves (slope of the curves in Fig. 4.8) become less dependent on the viscosity of the intermediate polymer zone as the initial separation between the waves decreases as seen by a comparison of the left and right branches near the end of each calculation. This reflects the fact that the effective mobility ratio of these waves tends towards that of the composite wave as the separation between these waves goes to zero (see Fig. 4.6). Thus one predicts that the growth rate of the S-wave will increase from its initial value and eventually approach a constant rate. One expects the same tendency for the C-wave, though the effect will be much milder (Figs. 4.7, 4.8). Results shown in Figs. 4.4–4.8 were obtained with 40×40 elliptic grid and 20×20 hyperbolic grid. When we increased the above grid numbers in Fig. 4.4 by two-fold, we did not find an appreciable change in the results. We did notice that the growth rate of the C wave slightly increased under mesh refinement, with the run being otherwise basically the same.

We briefly address the recovery efficiency of the polymer flood. Figure 4.9 plots the saturation (s^{**}) that would develop behind the composite, consisting of interacting

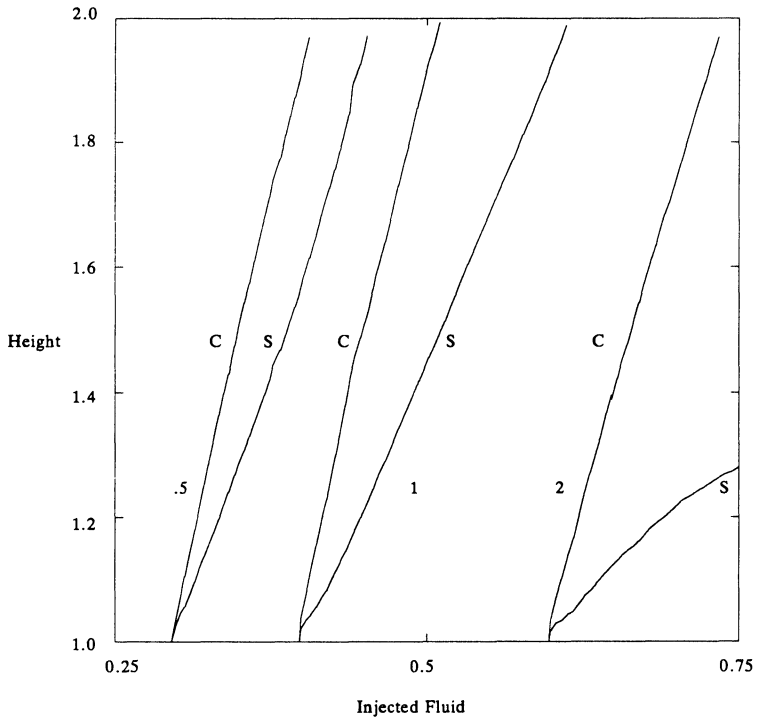

FIG. 4.7. *Effect of separation on stability: finger height (normalized wrt wavelength) of the S- and C-shocks as a function of injected fluid for different values of initial separation between the two interfaces. The viscosity ratio from bottom to top layer is* 1:6:10.

S- and *C*-waves in the limit of zero separation, as a function of the viscosity (ν_{wp}) of the (thin) intermediate polymer-thickened aqueous layer. Also plotted is the saturation (s^*) developed behind a leading isolated *S*-wave. The plots are given for two values of the viscosity ratio ν_w/ν_0. See Fig. 3.1 where s^{**} is the saturation of U^{**} and s^* is the saturation of the state U^*. The point to be stressed here is the following: the recovery effects of polymer strips are much better than that for continued injection of polymer-thickened water. In the continuous polymer injection case, a rarefaction fan trailing behind the leading *S*-wave will continue to sweep oil from behind the leading front and slowly raise local values from s^*. However, the effect is a very slow one, and economically costly. In contrast to this, the polymer strip provides a piston-like displacement up to a saturation value $s^{**} > s^*$. The question to be answered by computer calculations of reservoir flows modelling polymer floods is how well such polymer regions are retained in more realistic 2 and 3 dimensional flood situations, taking into account various additional phenomena such as polymer adsorption to the rock, polymer degradation, reservoir heterogeneities, etc.

4.2. Quarter five-spot floods—homogeneous media. The nonlinear wave coupling and interaction effects mentioned in the previous section can be used to enhance oil recovery. To demonstrate this, we considered various flooding processes in a quarter five-spot problem. In the quarter five-spot problem, the injection and production wells are at opposite corners of a diagonal of a rectangular domain. The domain is in the horizontal plane so there is no gravitational effect. We have carried out numerical experiments with three kinds of polymer flooding processes, namely (1) injection of polymer-water followed by pure water; (2) injection of pure water followed by

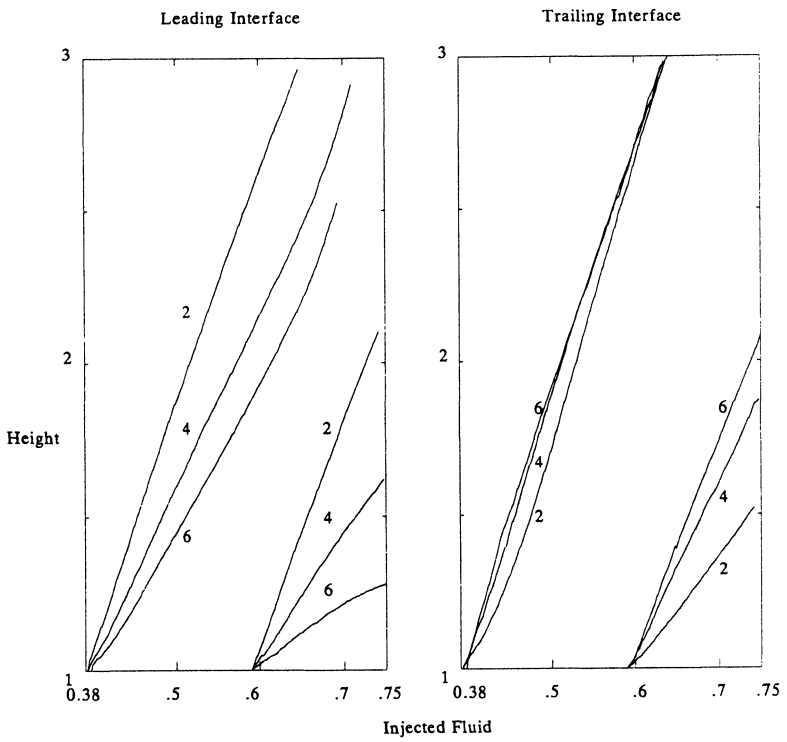

FIG. 4.8. *Effect of viscosity of the intermediate polymer-water layer on stability: finger height (normalized wrt to wavelength) of the leading* (a) *and the trailing* (b) *interfaces as a function of injected fluid for different values of the viscosity of the intermediate polymer layer. The initial dimensionless separation between the two interfaces is* 1 *for the left branch and* 2 *for the right branch in each of the above figures. The viscosities of the bottom and top layers are* 1 *and* 10, *respectively.*

polymer-thickened water and finally (3) injection of only polymer-water. The third case reduces to the Buckley-Leverett case with a modified value of water viscosity. We have kept the viscosity ratio of pure oil and water fixed at 10:1 in all our runs.

Figure 4.10 shows the temporal evolution of the S- (leading front) and the C- (trailing front) waves in the case when injection of polymer-thickened water is followed by pure water. The calculation is initialized at $t=0$ with the completely injected polymer-thickened aqueous slug present as an idealized annulus surrounding a small disk of pure water. The calculation proceeds with continued injection of pure water. In the calculation shown in Fig. 4.10 the viscosity ratio of the polymer-thickened aqueous zone to the pure water is $\nu_{wp} : \nu_w = 2:1$. As in the core flood studies, the leading interface is actually an S-family shock and a C-family contact discontinuity travelling with exactly equal velocities, and as before will behave exactly as an S family shock as long as the fluid ahead of the shock remains pure oil. If a backflow region occurs, the two shocks split and the calculation continues to track the S-wave as the two move apart. This does not occur in the homogeneous quarter five spot calculations done here. The trailing interface separating the polymer-thickened water from pure water is a C-family contact discontinuity.

As these two waves evolve, the C-wave moves faster than the S-wave as predicted in § 4.1 and the intermediate layer stretches and shrinks in width. In the calculation shown, the C-wave is unable to catch up with the S-wave, before the S-wave breaks

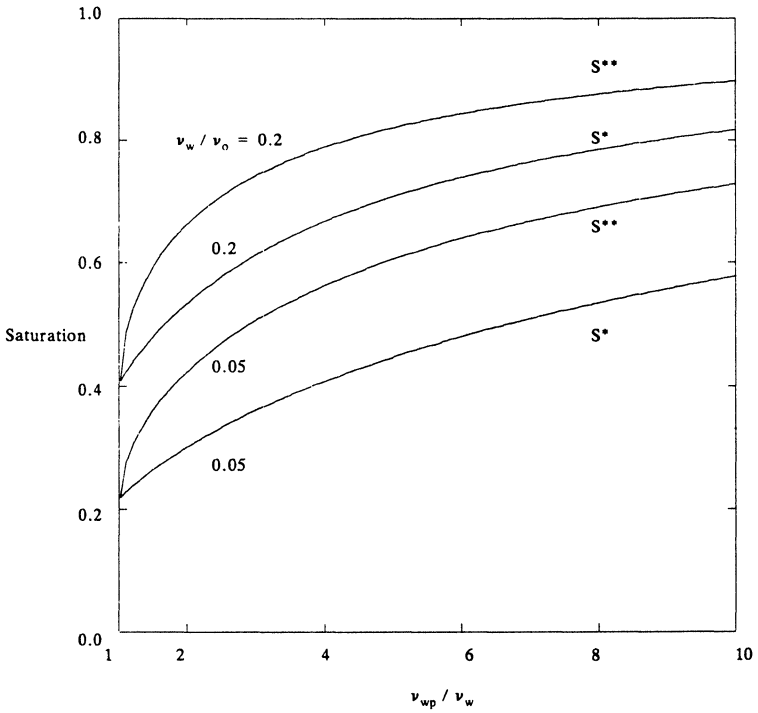

FIG. 4.9. *Saturation behind the S-wave (S*) and the composite wave (S**) as a function of the viscosity of the intermediate polymer zone for two different values of the viscosity ratio of the bottom (water) to top (oil) layer.*

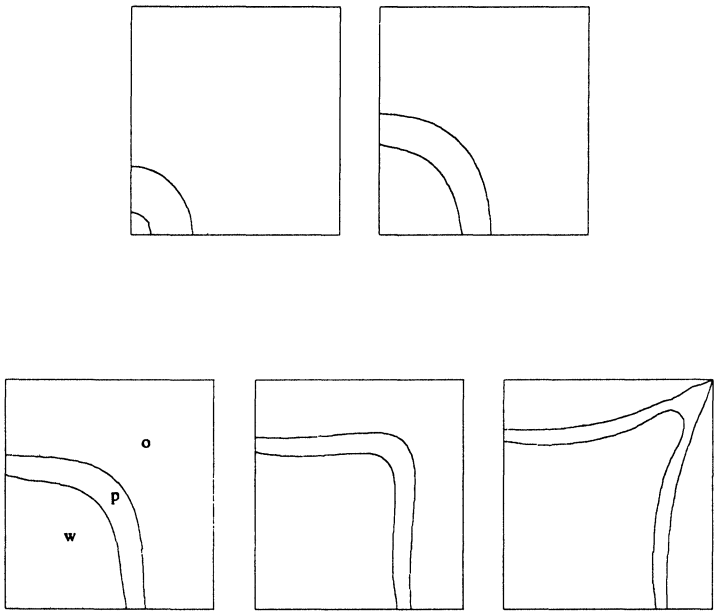

FIG. 4.10. *Temporal evolution of the leading shock (composed of S- and C-shocks) and the trailing C-shock. The initial viscosity ratio of pure water (w), polymer thickened water (p), and pure oil (o) is* 1:2:10.

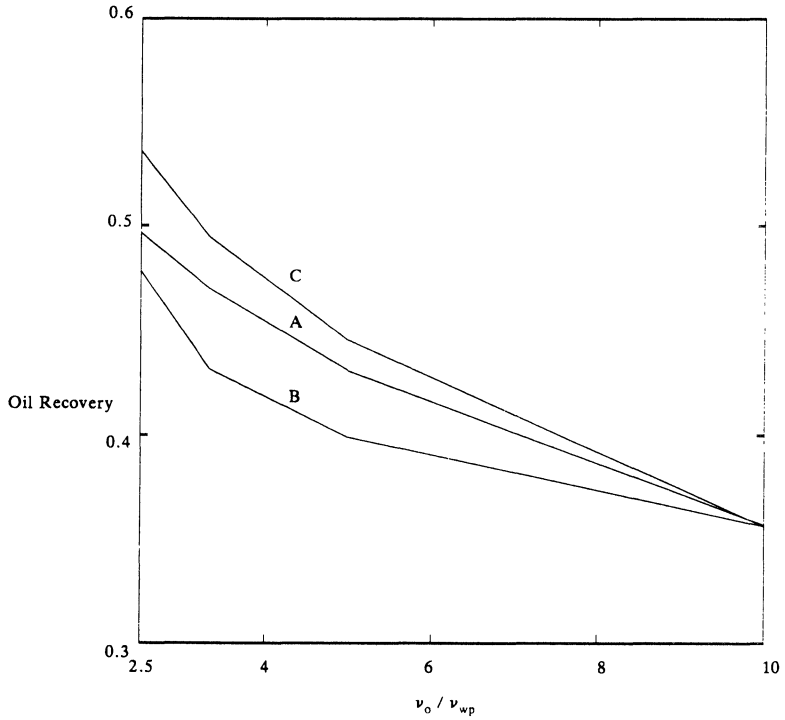

FIG. 4.11(a). *Fractional oil recovered at breakthrough as a function of the viscosity ratio* ν_0/ν_{wp} *for various processes:* (A) *polymer-thickened water followed by pure water* (B) *pure water followed by polymer-thickened water* (C) *only polymer-thickened water.*

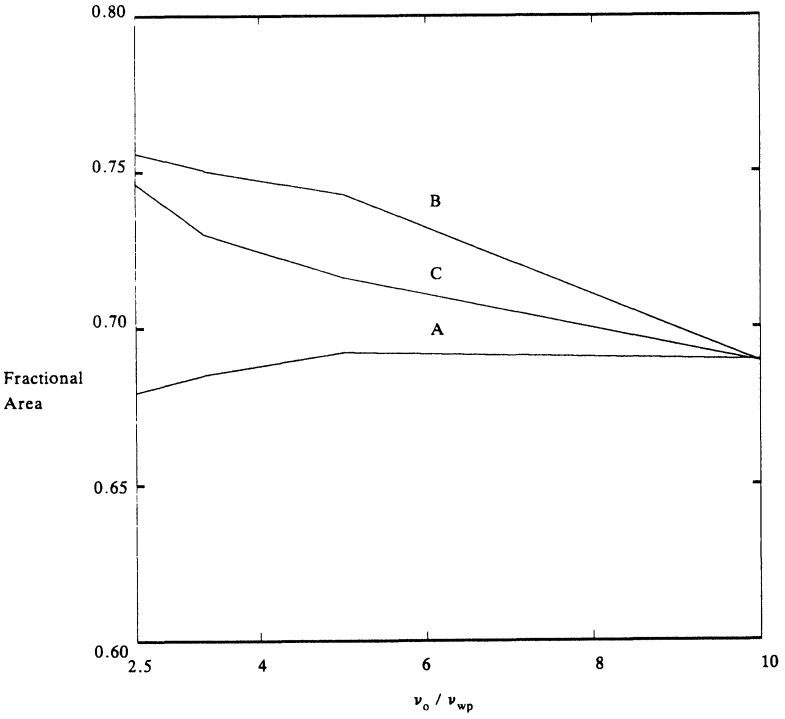

FIG. 4.11(b). *Fractional area swept by the leading front at breakthrough as a function of the viscosity ratio* ν_0/ν_{wp} *for various processes:* (A) *polymer-thickened water followed by pure water* (B) *pure water followed by polymer-thickened water* (C) *only polymer-thickened water.*

through at the production well. As an increase in ν_{wp} has a stabilizing effect on the S-wave and a destabilizing effect on the C-wave (Fig. 4.8), the breakthrough time for the S-wave will increase with the increase in ν_{wp}. This is indeed observed. In Fig. 4.11 we have plotted the net oil recovered at breakthrough (Fig. 4.11(a)) and the fractional area swept by the ahead front (Fig. 4.11(b)) as a function of the ν_{wp}. The fractional area swept by the leading front does not vary significantly with ν_{wp} (notice the compressed range of the y-axis). Presumably the reason for this is the small separation between the fronts and consequently the small amount of polymer injected. However the net oil recovered increases with ν_{wp} since an increase in ν_{wp} increases the piston-like displacement efficiency of the S-wave, as evidenced by the increase in the value of saturation s^* directly behind the S-wave.

4.3. Quarter five-spot floods—heterogeneous media. In all the runs mentioned above, the reservoir was homogeneous and the conclusions pertain purely to the effect of the nonlinear waves in the polymer-flooding process. Since the presence of polymer in the aqueous phase also inhibits the growth rate of fingers, one may expect the oil recovery in heterogeneous reservoirs to be increased (when compared to pure water flooding) due to both the effect of nonlinear waves and due to the control of fingering. Figure 4.12 shows a time sequence of an S-wave for the Buckley-Leverett case. The regions of local maxima (minima) of the rock permeability field are denoted by $+$ ($-$) signs. The variation in the permeability is "moderate." The injected fluid here is pure water; the viscosity ratio of the water to oil is 1:10. Notice that the fingering instability is initiated by the heterogeneity in the rock permeability. The fingering starts at the points of local maxima of the transmiscibility. This calculation was repeated with differing initial concentrations of polymer added to the water. The S-wave at

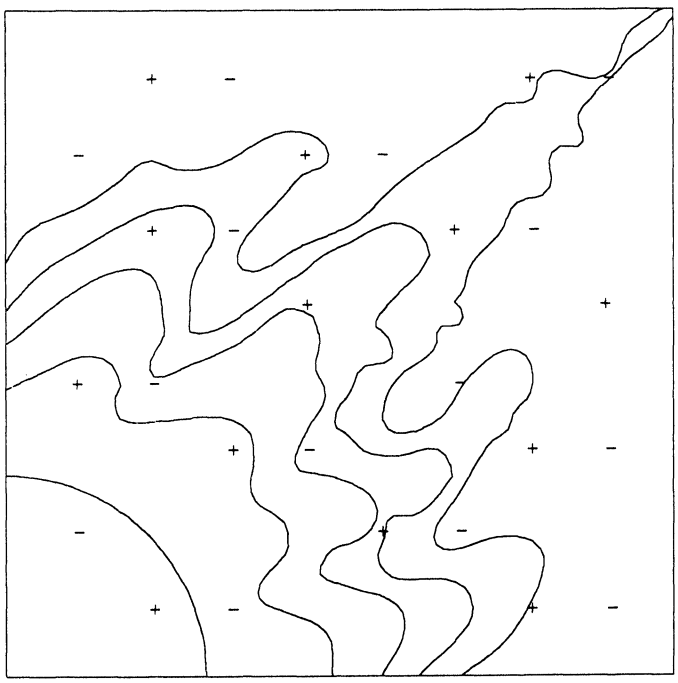

FIG. 4.12. *Growth of fingers for immiscible displacement in a heterogeneous reservoir: the temporal evolution of the Buckley-Leverett S-shock. The* $+$ ($-$) *signs correspond to local maxima (minima) of the permeability field. The viscosity ratio of the water to oil is* 1:10. *The elliptic grid is* 100×100, *the hyperbolic grid is* 50×50.

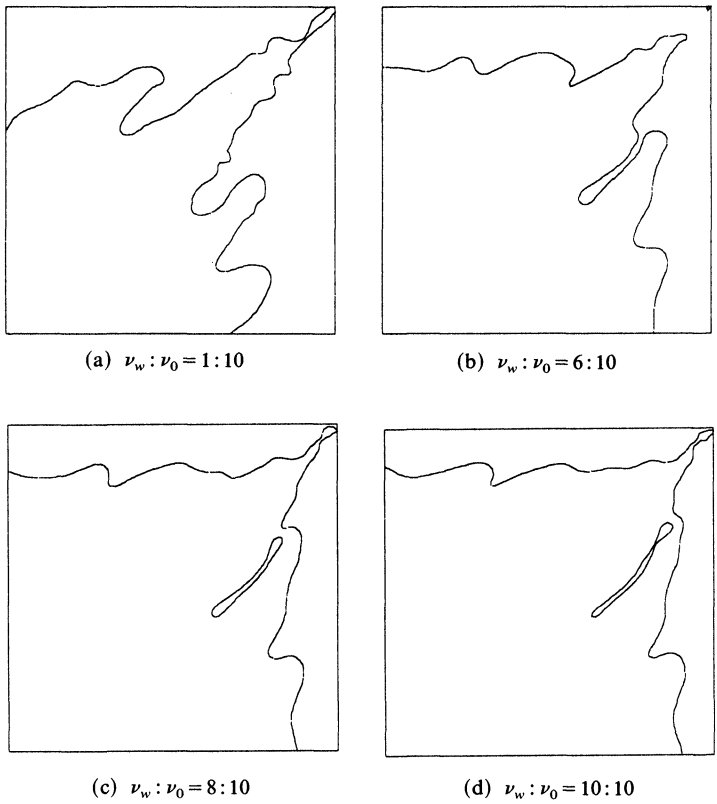

FIG. 4.13. *Effect of polymer in suppressing finger growth for immiscible displacement: the front position at breakthrough for various levels of concentration of polymer in water. The viscosity ratio across the front is given for each frame. The elliptic grid is* 100×100 *and the hyperbolic grid is* 50×50.

breakthrough is shown in Fig. 4.13 for four different levels of polymer concentration. The polymer has a dramatic effect in reducing the fingering growth rate. Also notice that at higher levels of polymer concentration a bifurcation in the topology of the tracked S-wave occurs, producing a region of by-passed oil. A mechanism for the entrapment of such oil pockets by the interface is the following: the front is stable for large polymer-water viscosities, leading to the merging (by a "pinching together" movement) of any fingers which may form due to the heterogeneous permeability. See the line drive calculations of [22] for a more detailed analysis of this problem.

In Fig. 4.14(a) we contrast the oil recovery at breakthrough as a function of the ratio of the displacing fluid viscosity to the oil viscosity for a homogeneous reservoir and for the heterogeneous reservoir calculations described above. Figure 4.14(b) plots the fractional area swept by the front as a function of the viscosity ratio for the homogeneous and heterogeneous calculations. One can see from these figures that reservoir heterogeneity indeed degrades oil recovery, and that polymer flooding can overcome the deleterious effects of the heterogeneity through an increase in the effective water viscosity. This conclusion is relevant only for the specific heterogeneity of Fig. 4.12, and further studies, including an analysis of discontinuous changes in the permeability field due to faults, shale and carbonate cement barriers, would be desirable.

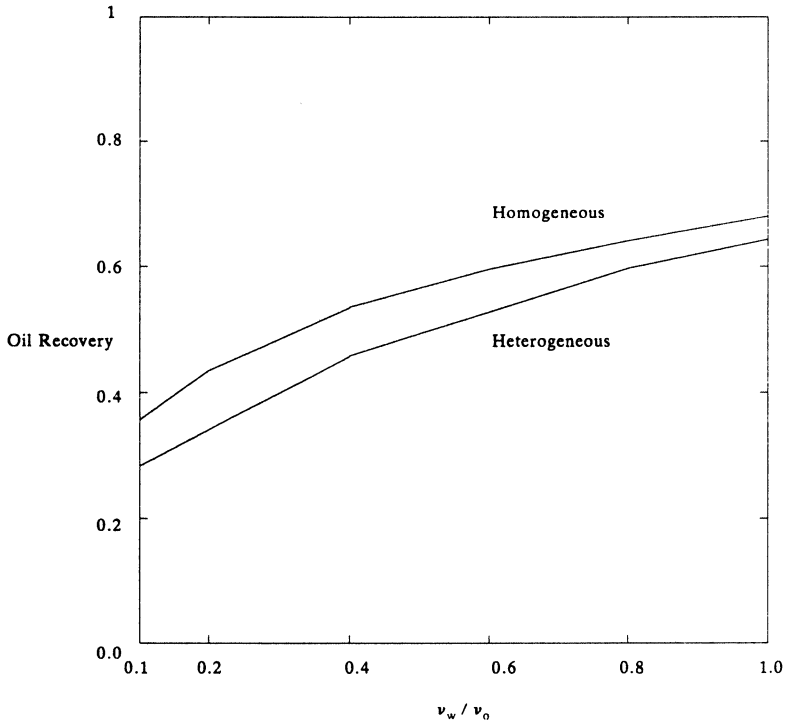

FIG. 4.14(a). *Fractional oil recovered at breakthrough as function of viscosity ratio of the behind fluid (polymer-thickened water) to the ahead fluid (oil) for heterogeneous and homogeneous reservoirs.*

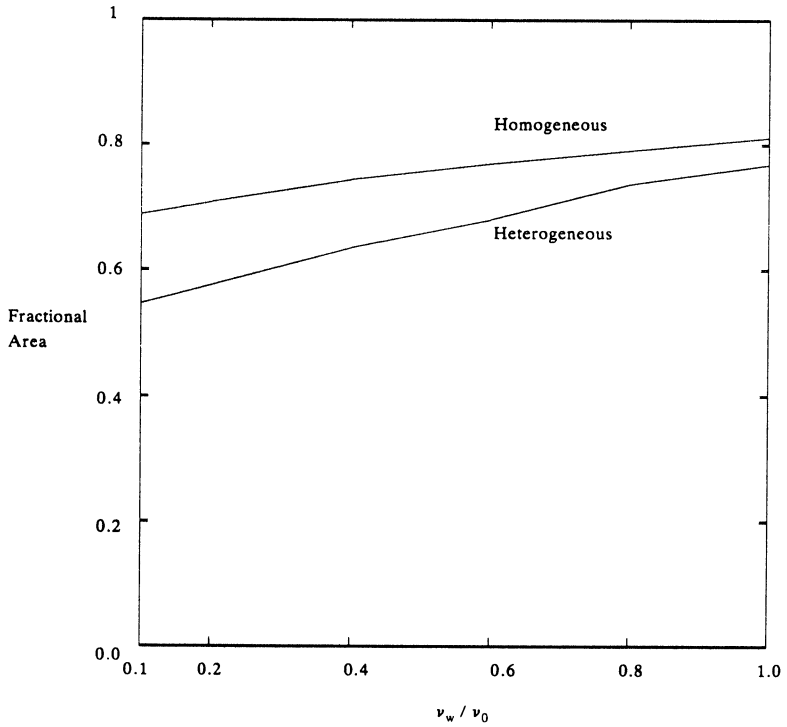

FIG. 4.14(b). *Fractional area swept by the front as function of viscosity ratio of the behind fluid (polymer-thickened water) to the ahead fluid (oil) for heterogeneous and homogeneous reservoirs.*

REFERENCES

[1] P. G. SAFFMAN, *Viscous fingering in Hele-Shaw cells*, J. Fluid Mech., 173 (1986), pp. 73-94.

[2] J. W. MCLEAN AND P. G. SAFFMAN, *The effect of surface tension on the shape of fingers in a Hele-Shaw cell*, J. Fluid Mech., 102 (1981), pp. 455-469.

[3] L. A. ROMERO, *The fingering problem in a Hele-Shaw cell*, Ph.D. thesis, California Institute of Technology, Pasadena, CA, 1981.

[4] D. A. REINELT AND P. G. SAFFMAN, *The penetration of a finger into a viscous fluid in a channel and tube*, SIAM J. Sci. Statist. Comput., 6 (1985), pp. 542-561.

[5] H. AREF AND G. TRYGGVASON, *Vortex dynamics of passive and active interfaces*, Phys. 12D (1984), pp. 59-70.

[6] G. R. BAKER, D. I. MEIRON AND S. A. ORSZAG, *Vortex simulation of the Rayleigh-Taylor instability*, Phys. Fluids, 23 (1980), p. 1485.

[7] ———, *Generalized vortex methods for free surface flow problems*, J. Fluid Mech., 123 (1982), pp. 477-501.

[8] P. CHARRIER AND B. TESSIERAS, *On front-tracking methods applied to hyperbolic systems of nonlinear conservation laws*, SIAM J. Numer. Anal., 23 (1986), pp. 461-471.

[9] I-L. CHERN, J. GLIMM, O. MCBRYAN, B. PLOHR AND S. YANIV, *Front tracking for gas dynamics*, J. Comp. Phys., 62 (1986), pp. 83-110.

[10] A. J. CHORIN, *The instability of fronts in a porous medium*, Comm. Math. Phys., 91 (1983), pp. 103-116.

[11] R. L. CHOUKE, P. VAN MEURS AND C. VAN DER POEL, *The instability of slow, immiscible viscous liquid-liquid displacement in permeable media*, Trans. AIME, 216 (1959), pp. 188-194.

[12] P. COLELLA AND M. BERGER, *Local adaptive mesh refinement for shock hydrodynamics*, submitted to J. Comp. Phys.

[13] A. J. DEGREGORIA AND L. W. SCHWARTZ, *A boundary-integral method for two-phase displacement in Hele-Shaw cells*, J. Fluid Mech., 164 (1986), pp. 383-400.

[14] J. GLIMM, D. MARCHESIN AND O. MCBRYAN, *Statistical fluid dynamics: unstable fingers*, Comm. Math. Phys., 74 (1980), pp. 1-13.

[15] ———, *Subgrid resolution of fluid discontinuities*, II, J. Comp. Phys., 37 (1980), pp. 336-354.

[16] J. GLIMM, E. ISAACSON, D. MARCHESIN AND O. MCBRYAN, *A shock tracking method for hyperbolic systems*, ARO Report 80-3, February 1980.

[17] J. GLIMM, D. MARCHESIN AND O. MCBRYAN, *A numerical method for two phase flow with an unstable interface*, J. Comp. Phys., 39 (1981), pp. 179-200.

[18] J. GLIMM, E. ISAACSON, D. MARCHESIN AND O. MCBRYAN, *Front tracking for hyperbolic systems*, Adv. in Appl. Math., 2 (1981), pp. 91-119.

[19] J. GLIMM, D. MARCHESIN AND O. MCBRYAN, *Unstable fingers in two phase flow*, Comm. Pure and Appl. Math., 34 (1981), pp. 53-75.

[20] J. GLIMM, B. LINDQUIST, O. MCBRYAN AND L. PADMANABHAN, *A front tracking reservoir simulator I: 5-spot validation studies and the water coning problem*, in Frontiers in Applied Mathematics, Vol. 1, Society for Industrial and Applied Mathematics, Philadelphia, PA, 1983.

[21] J. GLIMM, C. KLINGENBERG, O. MCBRYAN, B. PLOHR, D. SHARP AND S. YANIV, *Front tracking and two dimensional Riemann problems*, Adv. in Appl. Math., 6 (1985), pp. 259-290.

[22] J. GLIMM, J. GROVE, W. B. LINDQUIST, O. A. MCBRYAN AND G. TRYGGVASON, *The bifurcation of tracked scalar waves*, SIAM J. Sci. Statist. Comput., 9 (1988), pp. 61-79.

[23] J. GLIMM, O. MCBRYAN, R. MENIKOFF AND D. H. SHARP, *Front tracking applied to Rayleigh-Taylor instability*, SIAM J. Sci. Statist. Comput., 7 (1986), pp. 230-251.

[24] R. HOEGH-KRONE, *The Riemann problem in higher space dimensions*, Proc. of the IFE/SSI Conference on Reservoir Description and Simulation with Emphasis on EOR, Oslo, September 1986, and private communication.

[25] E. ISAACSON, *Global solution of a Riemann problem for a nonstrictly hyperbolic system of conservation laws arising in enhanced oil recovery*, J. Comp. Phys., to appear.

[26] T. JOHANSEN AND R. WINTHER, *The solution of the Riemann problem for a hyperbolic system of conservation laws modeling polymer flooding*, Institute for Energy Technology Preprint, to be published.

[27] G. R. JOHNSON, *Status of the EPIC Codes, Material Characterization and New Computing Concepts at Honeywell*, in Computational Aspects of Penetration Mechanics, Lecture Notes in Engineering, Vol. 3, Springer-Verlag, New York, 1983.

[28] B. KEYFITZ AND H. KRANSER, *A system of non-strictly hyperbolic conservation laws arising in elasticity theory*, Arch. Rational Mech. Anal., 72 (1980), pp. 219-241.

[29] R. KRASNY, *Desingularization of periodic vortex sheet roll-up*, J. Comput. Phys., 65 (1986), pp. 292-313.

[30] P. LAX, *Hyperbolic systems of conservation laws* II, Comm. Pure Appl. Math., 10 (1957), pp. 537-566.

[31] R. LAZARUS. Private communication.
[32] G. H. MCCALL, *A method for producing shockless acceleration of masses to hypervelocities using high explosives*, LaJolla Institute Preprint, LJI-TM-84-106, U. California at San Diego, May 1984.
[33] J. C. S. MENG AND J. A. L. THOMSON, *Numerical studies of some nonlinear hydrodynamic problems by discrete vortex element methods*, J. Fluid Mech., 84 (1978), pp. 433-453.
[34] R. MENIKOFF AND C. ZEMACH, *Rayleigh-Taylor instability and use of conformal map for ideal fluid flow*, J. Comput. Phys., 51 (1983), p. 28.
[35] G. MORETTI, *On the matter of shock fitting*, Proc. 4th Internat. Conference in Numerical Methods and Fluid Dynamics, Springer-Verlag, Berlin, 1975, pp. 287-292.
[36] W. F. NOH, *Artificial viscosity* (Q) *and artificial heat flux* (H) *errors for spherically divergent shocks*, Lawrence Livermore National Laboratory Preprint UCRL-89623, Livermore, CA, 1983.
[37] C.-W. PARK AND G. M. HOMSY, *The instability of long fingers in Hele-Shaw flows*, Phys. Fluids, 28 (1985), pp. 1583-1585.
[38] J. T. PATTON, K. H. COATS AND G. T. COLEGROVE, *Prediction of polymer flood performance*, Soc. Pet. Eng. J., (March 1971), pp. 72-84.
[39] C. S. PESKIN, *The fluid dynamics of heart valves: experimental, theoretical, and computational methods*, Ann. Rev. Fluid Mech., 14 (1982), pp. 235-259.
[40] B. PLOHR, *Modeling of shockless acceleration of thin plates using a tracked random choice method*, Los Alamos Preprint, Los Alamos National Laboratory, Los Alamos, NM, 1986.
[41] G. A. POPE, *The application of fractional flow theory to enhanced oil recovery*, Soc. Pet. Eng. J., (June 1980), pp. 191-205.
[42] W. PROSKUROWSKI, *A note on solving the Buckley-Leverett equation in the presence of gravity*, J. Comput. Phys., 41 (1981), pp. 136-141.
[43] R. D. RICHTMYER AND K. W. MORTON, *Difference Methods for Initial Value Problems*, Interscience, New York, 1967.
[44] B. E. RINGERS, *New Sliding Surface Techniques Enable Lagrangian Code to Handle Deep Target Penetration/Perforation Problems*, Computational Aspects of Penetration Mechanics, Lecture notes in Engineering, Vol. 3, Springer-Verlag, New York, 1983.
[45] B. K. SWARTZ AND B. WENDROFF, AZTEC: *A front tracking code based on Godunov's method*, Applied Numerical Mathematics, to appear.
[46] J. B. TEMPLE, *Global existence of the Cauchy problem for a class of* 2×2 *nonstrictly hyperbolic conservation laws*, Adv. Appl. Math., 3 (1982), pp. 335-375.
[47] G. TRYGGVASON AND H. AREF, *Numerical experiments on Hele-Shaw flow with a sharp interface*, J. Fluid Mech., 154 (1983), pp. 1-30.
[48] ———, *Finger interaction mechanisms in stratified Hele-Shaw flow*, J. Fluid Mech., 154 (1985), pp. 287-301.
[49] Y. ZHU AND B. CHEN, *A numerical method with high accuracy for calculating the interactions between discontinuities in three independent variables*, Scientia Sinica, 23 (1980).